Propagation of Fast Magnetoacoustic Waves in Stratified Solar Atmosphere*

ZHENG Hui-Nan(郑惠南)**, ZHANG Yuan-Yuan(张元元), WANG Shui(王水), WANG Chuan-Bing(王传兵), LI Yi(李毅)

CAS Key Laboratory for Basic Plasma Physics, School of Earth and Space Sciences, University of Science and Technology of China, Hefei 230026

(Received 20 September 2005)

The characteristics of magnetohydrodynamic fast wave propagation in the solar stratified atmosphere are studied by the ray tracing method. The propagation behaviour of the wavefronts is described in detail. A magnetic field incorporating the characteristics field spreading expected in flux tubes is used, which represents the main feature of an active region. Partly ionization is considered beside the stratified solar atmosphere consisting chromosphere, transition region and corona. The study may explain the characteristics in observations of Moreton and extra-ultraviolet image telescope (EIT) waves. The wavefront incurred by the disturbance initialized at the base of the transition region propagates fast initially due to strong magnetic field, and it slows down when arriving beyond the region of flux-tube. Meanwhile, the wave propagates in the corona with a more consistent speed, as seen in the observation of EIT waves. The speeds and propagated characteristics in chromosphere and corona of the wavefronts are in agreement with those observed in H_α Moreton and EIT waves, respectively.

PACS: 52. 30. Cv, 96. 60. −j

Moreton waves, which have been well studied since the early 1960s,[1] are recognized as some disturbances initiated by the explosive phase of flares and propagating through the solar atmosphere with speeds ranging from several hundreds to over one thousand $\mathrm{km{\cdot}s^{-1}}$. They are suggested to be magnetohydrodynamic (MHD) fast mode magnetoacoustic waves propagating in the chromosphere.[2] Extra-ultraviolet image telescope (EIT) waves, recently obtained by SOHO/EIT observations,[3,4] are related to the corona mass ejections (CME). They have been investigated by several authors who suggest that EIT waves be fast mode magnetoacoustic waves.[5,6]

These waves (Moreton waves and EIT waves) are presumed to be of the same type while propagating in different parts of the solar atmosphere.[7] To understand the characteristics of MHD waves propagating in the stratified solar atmosphere, several approaches have been performed by multi-dimensional MHD numerical simulations.[8−11]. However, all of the above-mentioned works have the defects in which the exact properties of the solar atmosphere in the active region are not incorporated. Moreover, a fast mode magnetoacoustic characteristic consistent with the observation in Moreton wave propagation can not be given in the one-fluid model since relative higher density and lower temperature result in both smaller sound and Alfvenic wave characteristics, then the smaller fast magnetoacoustic wave characteristic.

The observation shows that the stratified solar atmosphere is actually not fully ionized in the chromosphere and transition region.[12,13] We argue that partial ionization may play an important role in wave propagation. In order to further investigate the wave characteristics in a partly ionized fluid, a multi-fluid MHD model is required to study the related dispersion relation. A two-fluid MHD model is adopted here, in which two species consisting are neutral (hydrogen) and ionized (proton and electron) gases. MHD equations can be deduced on the basis of the literature,[14−16] and for simplicity, only the collision effect is considered here. The deduced equations are written as follows:

$$\frac{\partial n_A}{\partial t} + \nabla \cdot (n_A \boldsymbol{u}_A) = 0, \tag{1}$$

$$\frac{\partial p_A}{\partial t} + \boldsymbol{u}_A \cdot \nabla p_A + \gamma p_A \nabla \cdot \boldsymbol{u}_A = 0, \tag{2}$$

$$\frac{\partial \boldsymbol{u}_A}{\partial t} + \boldsymbol{u}_A \cdot \nabla \boldsymbol{u}_A + \frac{1}{n_A m_A}\nabla p_A - \boldsymbol{g} = \nu(\boldsymbol{u}_B - \boldsymbol{u}_A), \tag{3}$$

$$\frac{\partial n_B}{\partial t} + \nabla \cdot (n_B \boldsymbol{u}_B) = 0, \tag{4}$$

$$\frac{\partial p_B}{\partial t} + \boldsymbol{u}_B \cdot \nabla p_B + \gamma p_B \nabla \cdot \boldsymbol{u}_B = 0, \tag{5}$$

$$\frac{\partial \boldsymbol{u}_B}{\partial t} + \boldsymbol{u}_B \cdot \nabla \boldsymbol{u}_B + \frac{1}{n_B m_B}\nabla p_B - \frac{1}{4\pi n_B m_B}(\nabla \times \boldsymbol{B}) \times \boldsymbol{B} - \boldsymbol{g} = \nu(\boldsymbol{u}_A - \boldsymbol{u}_B), \tag{6}$$

$$\frac{\partial \boldsymbol{B}}{\partial t} = \nabla \times (\boldsymbol{u}_B \times \boldsymbol{B}), \tag{7}$$

where subscripts A and B specify neutral (hydrogen) and ionized (proton and electron) gases, respectively; ν is the collision coefficient between two species. All the quantities have their usual meanings. The dispersion relation can then be retrieved by some general assumption as that in the one-fluid MHD model and

* Supported by the National Natural Science Foundation of China under Grant Nos 40274050 and 40336052, and the National Key Basic Research Special Foundation of China under Grant No G2000078405.

** Email: hue@ustc.edu.cn

expressed as

$$\begin{aligned}0 = D(\omega,k) &= \omega^3[(\omega-i\nu)(\omega^2-k^2b_n^2)-i\nu\omega^2]\\ &\times\{\omega(\omega-2i\nu)[\omega(\omega^2-k^2a^2)\\ &\cdot(\omega^2-k^2(a^2+b^2)-i\nu\omega)\\ &-i\nu(\omega^4-\omega^2k^2(a^2+b^2)+k^4a^2b_n^2)]\\ &-\omega k^2b_n^2(\omega^2-k^2a^2)(i\nu\omega-k^2a^2)\},\end{aligned}\tag{8}$$

where $a=\sqrt{\gamma RT_0}$ is the sound characteristic (two species of gas are assumed to have the same thermal properties with identical undisturbed temperature T_0), R is the gas constant, $b^2=\dfrac{B_0^2}{4\pi m_B n_{B0}}$ is the square of the Alfvenic wave characteristic in ionized gas, $b_n=b\cos\theta$ and θ is the angle between directions of wave propagation and undisturbed magnetic field. Subscript 0 represents the undisturbed quantities. One can easily seen that the dispersion relation reduces to that in two-fluid with no collision when $\nu=0$, namely, the decoupled dispersion relations for hydrodynamics and magnetohydrodynamic gases.

To question the wave modes with collision effect in consideration, Eq. (8) can be rewritten as

$$\begin{aligned}0 = D(\bar\omega,\bar k) &= \bar\omega^3[(\bar\omega-i)(\bar\omega^2-\bar k^2s\cos^2\theta)-i\bar\omega^2]\\ &\times\{\bar\omega(\bar\omega-2i)[\bar\omega(\bar\omega^2-\bar k^2)(\bar\omega^2-\bar k^2(1+s)-i\bar\omega)\\ &-i(\bar\omega^4-\bar\omega^2\bar k^2(1+s)+\bar k^4s\cos^2\theta)]\\ &-\bar\omega\bar k^2s\cos^2\theta(\bar\omega^2-\bar k^2)(i\bar\omega-\bar k^2)\},\end{aligned}\tag{9}$$

where $\bar\omega=\omega/\nu$, $\bar k=ka/\nu$, and $s=b^2/a^2$. The typical dispersion relations are given in Fig. 1, with parameters $\cos\theta=b_n/b=0.5$. The results show that the fastest wave mode characteristic is slightly different from that in the collisionless situation except when $\omega/\nu\sim1$, where the fastest wave mode characteristic is the fast magnetoacoustic wave characteristic in the one-fluid MHD model with the plasma density equal to the ionized portion of the entire composition, though the frequencies and wave number may endure some restriction so that the wave may be damped. Detail studies (see Figs. 1(e)–1(f)) show that the scale of growth or damping is around $0\sim2\nu$, namely in the same order of collision frequency. In this study, growth or damping effect will not be discussed further in the calculation and hereafter, fast magnetoacoustic wave characteristic in ionized gas without collision will be used to carry out the further studies.

For better understanding of the characteristics of Moreton waves and EIT waves, observed in chromosphere and corona, respectively, a magnetic field is taken as in Refs. [17, 18], which incorporates the feature of field in the active region. The magnetic flux

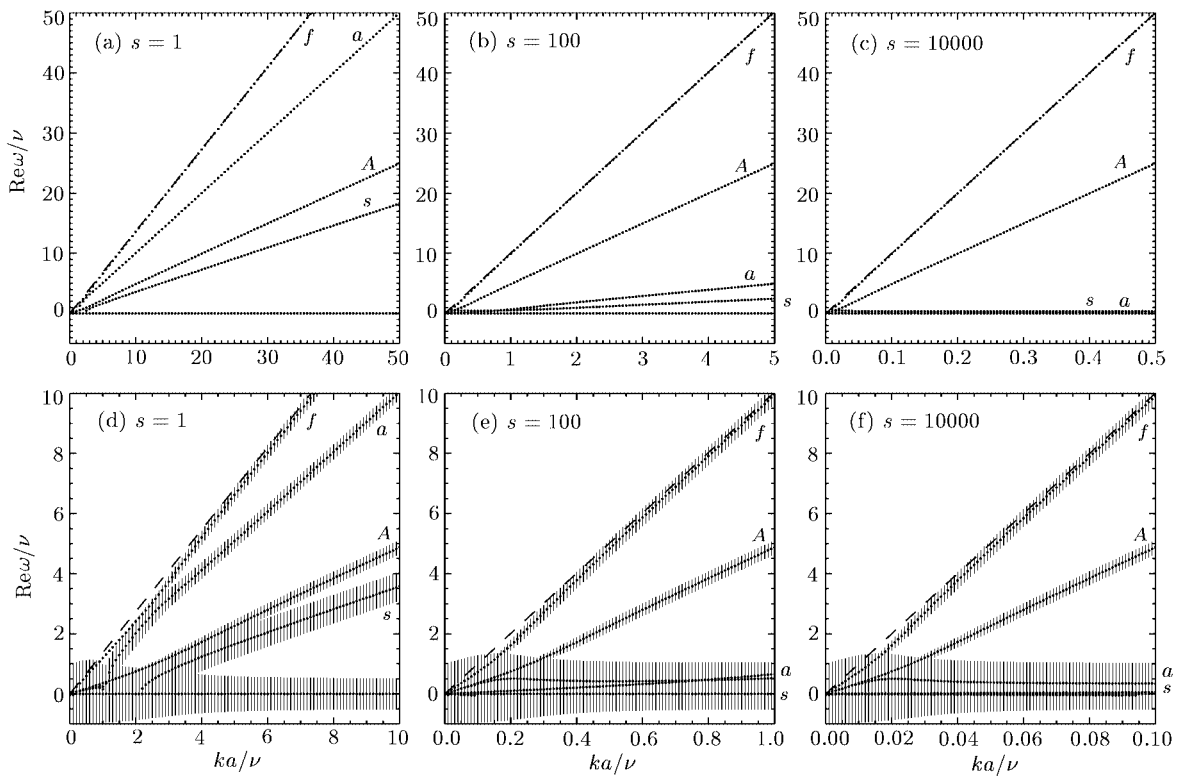

Fig. 1. Dispersion relations (with $\cos\theta=b_n/b=0.5$): (a) $s=1$, (b) $s=100$, and (c) $s=10000$; (d)–(f) detail with $0.0\le\omega/\nu\le10.0$ (error bars denote the amplitudes of ω_I, the imaginary part of ω), corresponding to (a)–(c), respectively. The dotted lines are the solutions to Eq. (9) and the dashed lines are those corresponding to the fast magnetoacoustic characteristics in the asymptotic limit ($\nu=0$). The dotted lines marked with a, A, s, and f correspond to the sound, Alfven, slow, and fast characteristic modes in the asymptotic limit ($\nu=0$), respectively. Trivial roots $\omega=0$ is also shown.

function is expressed as

$$A = B_0 \left\{ x + \sum_n \frac{C_n}{\pi n} \sin(n\pi x/L_0) \cdot \frac{\cosh[n\pi(\delta - z/L_0)]}{\cosh[n\pi(\delta - z_b)]} \right\}, \quad (10)$$

where B_0 is the field strength in the corona, $C_n = \frac{2\sin(n\pi\epsilon)}{n\pi\epsilon}$, L_0 the half characteristic width of the magnetic field, δ is the height in units of L_0, from which the magnetic field directs up strictly vertically. Moreover, a simplified model with two temperature gas layer is considered, similar to that in Ref. [9]. The distribution of the initial temperature is expressed as

$$T = \frac{1}{2}(T_{cor} + T_b) + \frac{1}{2}(T_{cor} - T_b) \cdot \tanh\left(\frac{2z}{\delta z_s} - \frac{z_t}{z_s}\right), \quad (11)$$

where T_{cor} and T_b are the temperatures in the corona and chromosphere respectively, z_t is the height of the base of the corona, z_s is the half scale height of temperature in the transition region. Hereafter, the plasma pressure and density can be deduced from hydrostatic and gas state equations. By considering partial ionization, the density consists of two parts, ionized and neutral. The ratio of ionized particles to the total one, according to the data in Refs. [12, 13], is modelled by the following:

$$\alpha = \frac{1}{2}(\alpha_{cor} + \alpha_b) + \frac{1}{2}(\alpha_{cor} - \alpha_b) \cdot \tanh\left(\frac{2z}{\delta z_s} - \frac{z_t}{z_s}\right). \quad (12)$$

An example of the magnetic field configuration, as well as the temperature, overall and ionized densities of gas are shown in Fig. 2. The half width of the magnetic field in a flux tube is chosen to be 30000 km so that it covers the active region in some extent.

One can see clearly in Fig. 2 that the magnetic field is strong in the neighbourhood of the centre at the bottom of the transition region and in the chromosphere. The field strength is much weaker and most evenly distributed far away from the active region. The magnitude of the field strength can be around 10 to 1000 or more times of that in a quite large region. The temperature changes rapidly from 1×10^4 K in the chromosphere to 1×10^6 K in corona. The overall density decreases in the order of 10^4 with the height from chromosphere to corona. Meanwhile ionized density is much less than that of the overall density in the transition region and in the chromosphere. The fastest wave mode characteristic speed is almost the same as that of fast MHD acoustic wave for ionized fluid from the prior studies of dispersion relation in this study, and therefore is approximately expressed by

$$c_f = \left\{ \frac{1}{2}[a^2 + b^2 + \sqrt{(a^2+b^2)^2 - 4a^2b_n^2}] \right\}^{\frac{1}{2}}, \quad (13)$$

as that in one-fluid MHD equations but with the ionized density. This gives a characteristic of the fastest wave mode in the transition region and chromosphere much larger than that derived in one-fluid MHD model.

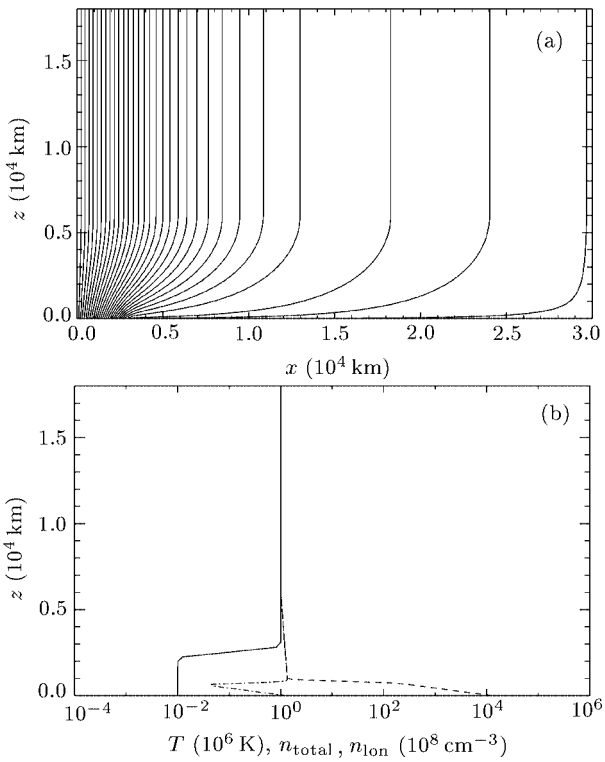

Fig. 2. (a) Magnetic field configuration consisting of active region. Total 1024 summations are taken in Eq. (10), and $L_0 = 3 \times 10^4$ km, $\epsilon = 0.1$, $\delta = 0.2$, $z_b = 0.0$. (b) Temperature (solid), overall (dashed) and ionized (dot-dashed) densities variation with height. The corresponding parameters are $z_t = 900$ km, $z_s = 50$ km, $T_{cor} = 10^6$ K, $T_b = 10^4$ K, $\alpha_{cor} = 1.0$, and $\alpha_b = 0.0001$. The data used here can be referred to Ref.[12].

According to the method of ray tracing method for MHD,[20] the equations of the wavefronts for the fast mode wave are described by

$$H_f = \boldsymbol{v} \cdot \boldsymbol{p} \pm c_f p, \quad (14)$$

$$\frac{d\boldsymbol{x}}{dt} = \frac{\partial H_f}{\partial \boldsymbol{p}} = \boldsymbol{v} \pm c_f \boldsymbol{n} \mp \frac{b^2(B_n/B^2)}{c_f C}(\boldsymbol{B} - B_n \boldsymbol{n}), \quad (15)$$

$$\frac{d\boldsymbol{p}}{dt} = \frac{\partial H_f}{\partial \boldsymbol{x}} = -(\boldsymbol{p} \cdot \nabla)\boldsymbol{v} - \boldsymbol{p} \times (\nabla \times \boldsymbol{v}) \mp p \nabla c_f, \quad (16)$$

which are the canonical equations for motion of the wavefront. Here $\boldsymbol{x}$ and $\boldsymbol{p}$ are the wave front position and the wave normal, respectively. $C = [(1+s)^2 - 4s\cos^2\theta]^{1/2}$ and $s = b^2/a^2$.

To study the propagation of the wave, a line disturbance is introduced in the center of magnetic field in the neighbourhood of the corona base. Equations (15) and (16) are solved numerically by a second-order Runge–Kutta finite difference method for ordi-

nary differential equations. For simplicity, we assume $\boldsymbol{v} = 0$. Computations with different parameters have been performed but only one of the results with appropriate set of parameters will be given here, which is close related in quality to that of a well understood observation,[21] and discussed in the following.

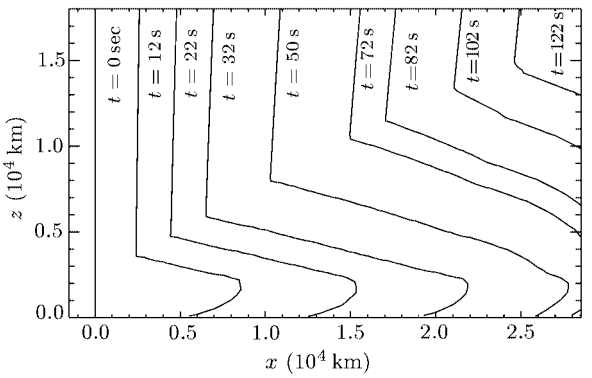

Fig. 3. Wavefront evolving with time. The disturbance is imposed at the centre of the active region ($x = 0$). The ambient magnetic field has the same parameters as that in Fig. 2, except $\delta = 0.8$, which produces that the ratio of the fastest characteristic of fast mode in chromosphere to that in corona is roughly 3.

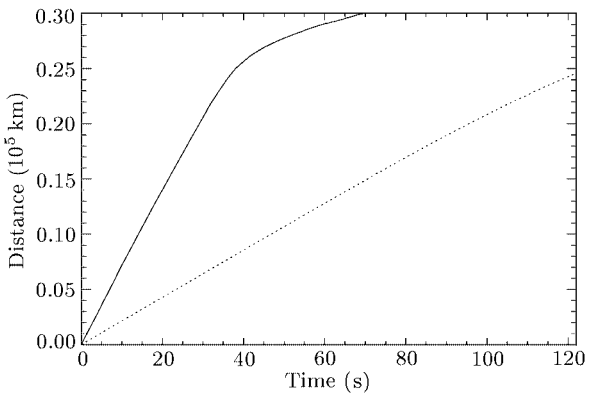

Fig. 4. Locations of wavefronts from Fig. 3 in the corona and chromosphere with time. Solid and dashed lines are (horizontal) wave front propagation distances from the disturbing source. Propagation speed in the chromosphere is estimated by the farthest position of wave front in the chromosphere, and that in the corona by the front position in the height of 15000 km.

The calculated results of the wavefront diagram evolving with time are shown in Fig. 3. The initial magnetic field chosen here has a smoother change overall in which the maximum of fast mode characteristic in the transition region/chromosphere is roughly 3 times of that in the corona. It can be seen from the figure that nearby the position where the disturbance is imposed, the wavefront moves faster in the transition region and chromosphere where strong magnetic field dominates. Meanwhile the wavefront in the corona progresses away from the disturbance in a mostly constant speed. When the wave propagates far away from the active region, it slows down in the transition region and chromosphere but its counterpart in the corona moves steadily as before. Furthermore, the locations of the wave fronts initially locating in the chromosphere and corona with time are shown in Fig. 4. Propagation speed in the chromosphere is estimated by the farthest position of wave front in the chromosphere, and that in the corona by the front position in the height of 15000 km. The estimated propagating speeds are consistent with those of the Moreton and EIT waves by observation, which are approximately 715 kms^{-1} and 202 kms^{-1}, respectively.[21] This model, as suggested in Ref. [9], additionally with the assumption of partly ionized gas in the transition region and chromosphere, gives the required non-uniformity of the wave propagation speeds. The wavefronts in the chromosphere decelerate rapidly when it moves away from the active region where strong magnetic field dominates. One may have noted that EIT waves cover a wider angular span. They were also observed to be far away from the flare site more than the Moreton waves. This is probably due to slowdown of Moreton waves before they were observed by EIT, though some argued that this may be precluded by the oscillations of a remote filament, for which Moreton waves were responsible for.[22] The present study also suggests that the Moreton waves dissipate while they are propagating away in the order of collision frequency, which provides a possible explanation that the Moreton waves cover a smaller region.

References

[1] Moreton G E 1960 *Astron.* J. **65** 494
[2] Uchida Y 1968 *Solar Phys.* **4** 30
[3] Plunkett S P et al 1998 *Geophys. Res. Lett.* **25** 2477
[4] Thompson B J et al 1998 *Geophys. Res. Lett.* **25** 2465
[5] Wang Y M 2000 *Astrophys. J. Lett.* **543** L89
[6] Wu S T et al 2001 *J. Geophys. Res.* **106**:A11 25089
[7] Thompson B J et al 2000 *Solar Phys.* **193** 161
[8] Zheng H N, Wang S, Wu S T and Li B 2001 *Chin. Phys. Lett.* **18** 1624
[9] Li B, Zheng, H N and Wang S 2002 *Chin. Phys. Lett.* **19** 1639
[10] Zheng H N, Wang S and Li B 2003 *Stellar Astrophysics—A Tribute to Helmut A. Abt* ed Cheng K S, Leung K C and Li T P (Dordrecht: Kluwer) p 301
[11] Chen P F, Wu S T, Shibata K and Fang C 2002 *Astrophys. J.* **572** L99
[12] Vernazza J E, Avrett E H and Loeser R 1981 *Astrophys. J. Suppl.* **45** 635
[13] Lin Y Z 2000 *Introduction to Solar Physics* (Beijing: Science Press) pp 133 274 313
[14] Schunk R W 1975 *Planet. Space Sci.* **23** 437
[15] Judge P G and Peter H 1998 *Space Sci. Rev.* **85** 187
[16] Lenz D D 1999 *Astrophys.* J. **517** 497
[17] Athay R G 1981 *Astrophys.* J. **249** 340
[18] Cargill P J, Spicer D S and Zalesak S T 1997 *Astrophys. J.* **488** 854
[19] Shibata K et al 1989 *Astrophys. J.* **345** 584
[20] Jeffrey A and Taniuti T 1964 *Non-linear Wave Propagation with Application to Physics and Magnetohydrodynamics* (New York: Academic) pp 40 184
[21] Eto S et al 2002 *Publ. Astron. Soc. Jpn.* **54** 481
[22] Narukage N et al 2002 *Astrophys. J.* **572** L109